FOREX Publication
Open Access | Rapid and quality publishing

International Journal of
Electrical and Electronics Research (IJEER)
Research Article | Volume 14, Issue 2 | Pages 343-350 | e-ISSN: 2347-470X

A Geometrically Reconfigurable Patch Antenna with Resonant-Mode Control for CubeSat Communications

Baydaa Ali Ismail[1], and Israa Hazem Ali[2]

[1]Department of Communications, College of Engineering, University of Diyala, Diyala, Iraq; Email: eng_grad_communication2504@uodiyala.edu.iq
[2]Department of Communications, College of Engineering, University of Diyala, Diyala, Iraq; Email: israa hassan eng@uodiyala.edu.iq

***Correspondence:** *Email:* e *eng_grad_communication2504@uodiyala.edu.iq*; *Tel.: +9647726902179*

ABSTRACT– Compact and effective antenna designs are needed to meet the radiation stability, lightweight, and compactness criteria of CubeSat communication systems. This study presents a CST Studio Suite-optimized tiny single-layer microstrip patch antenna for X-band CubeSat applications. In order to improve radiation performance and impedance matching without adding more structural complexity, a novel method incorporating resonant-mode control *via* geometric reshaping is suggested. With a directivity of 5.24 dBi and 6.38 dBi, respectively, and a reflection coefficient (S_{11}) of −20.06 dB at 11.347 GHz and −54.92 dB at 12.809 GHz, the first antenna design exhibits dual-band performance. This setup can be modified to eliminate the lower-order mode and produce a single-band response at 12.232 GHz with improved directivity of 9.30 dBi and S_{11} of −32.97 dB by changing the feed line and deleting the lateral patch frame. The findings demonstrate that an antenna can shift from a dual-band operation to a high-directivity single-band operation within the same antenna construction by systematically manipulating the resonant modes through controlled geometric adjustments. For dependable X-band CubeSat communication systems, the suggested architecture is low profile, structurally straightforward, and effective.

Keywords: Microstrip patch antenna, X-band, Gain, Cubesat, Directivity.

ARTICLE INFORMATION
Author(s): Baydaa Ali Ismail and Israa Hazem Ali;
Received: 06/01/26; **Accepted**: 29/05/26; **Published**: 20/06/26;
E- ISSN: 2347-470X;
Paper Id: IJEER260101;
Citation: 10.37391/ijeer.140210
Webpage-link:
https://ijeer.forexjournal.co.in/archive/volume-14/ijeer-140211.html

1. INTRODUCTION

Modern communication systems rely heavily on wireless communication, which allows dependable data exchange without the use of physical transmission media. In particular, satellite communication (SATCOM) is crucial for supplying access to underserved and rural areas with little or no terrestrial infrastructure. For example, a single geostationary satellite may cover a wide geographic region, which makes satellite systems very useful for global communication services, broadcasting, and remote sensing [1],[2]. CubeSats are often used in Low Earth Orbit (LEO) due to shorter development times and reduced costs of launch. In the case of complex communication services, they cover a lot of bandwidth, VHF/ UHF to high-capacity K, Ku, and Ka bands [3],[4]. They are prohibited by small space, power budget, antenna aperture, and demand of reliable deployment and connection performance, but the small size, lightweight structure, and COTS-based design enable fast and low-cost deployment [5]. Because of its lightweight design, ease of production, low profile, and compatibility with planar integration, microstrip patch antennas are frequently utilized in CubeSat systems[6],. Despite these benefits, they have intrinsic drawbacks such poor gain, restricted bandwidth, and decreased radiation efficiency[7]. Therefore, one of the most important research challenges is to improve their performance without increasing structural complexity[8]. M. I. Hasan et al. proposed in 2025 to develop a circularly polarized X-band microstrip antenna with a ring of 16 mushroom-shaped electromagnetic band-gap (EBG) elements in order to improve radiation performance and reduce the amount of surface waves. To generate right-hand circular polarization, the patch was etched with two diagonal square patches. The antenna had a gain of 11.7 dBi at 8.48GHz. This outcome shows how well the EBG setup enhances radiation characteristics. The described reflection coefficient of S_{11}= -18.18 dB at the same frequency further proved an appropriate matching level. However, because input-impedance behavior and VSWR characteristics were not provided by the research, there are certain gaps in the evaluation of the overall matching performance [9]. In 2025, Tanna and Rathod devised a larger Ka-band patch antenna (microstrip) for CubeSat applications 0with 21 circular holes in the patch borders and parasitic elements to increase the impedance bandwidth and gain. It was discovered that the initial inset-fed structure functioning at 26.4 GHz with an impedance bandwidth of 18% and S11 = -20.6 dB was successful. A secondary resonance at 27.7 GHz with a 20.7% wider bandwidth and an enhanced S11 of -38.5 dB was produced by adding a parasitic component. After slot loading, the operating frequency was adjusted to 28.3 GHz, resulting in an operational

FOREX Publication
Open Access | Rapid and quality publishing
International Journal of Electrical and Electronics Research (IJEER)
Research Article | Volume 14, Issue 2 | Pages 343-350 | e-ISSN: 2347-470X

bandwidth of 21.5% and an augmented gain of 7 dBi. S11 = -40.14 dB was the final stage's reflection coefficient. Also, input-impedance behavior and VSWR characteristics were not mentioned in the study, which restricted a detailed analysis of the matching performance over the operating range[1]. In order to improve impedance matching and bandwidth performance, Marco Simone et al. built a Ka-band stacked CubeSat communication at microstrip patch antenna in 2021 using particle swarm optimization (PSO). With a gain of almost 8 dBi, the optimized single-element architecture (bandwidth 5.53 GHz at 33.185 GHz) demonstrated a significant improvement over the traditional stacked-patch system. The antenna's high gain of about 26 dBi was increased to an 8x8 stacked array, demonstrating the antenna's suitability for large-capacity CubeSat downlink communication applications. However, given the stringent constraints of CubeSat platforms, the implementation relies on two radiating components, increasing the total number of components required and potentially increasing the cost of fabrication and mechanical assembly complexity[10]. In 2023, Pittella et al. presented a tiny S-band patch antenna device built of 3D-printable materials that was fully compatible with standard CubeSat configurations. Considering the mass and size constraints of the CubeSat, the antenna was designed and computationally analyzed in an electromagnetic computer-aided design (CAD) environment using polylactic acid (PLA) as the substrate. The computed S-parameters demonstrate exceptional impedance-matching performance with a deep resonance at 2.45 GHz with a S_{11} of roughly −32 dB. The system functions within the ITU amateur satellite allocation of 2.40–2.45 GHz. Furthermore, the footprint is kept small enough for direct surface integration on CubeSat modules. However, the study only included the directivity radiation plot, which is an essential statistic for assessing the antenna's actual radiated performance; the associated gain pattern was not[11] . In 2023, Kumar et al. introduced a small three-band microstrip patch antenna for satellite communication. It combined a half-circular radiating patch with a defective ground structure (DGS) to achieve wide impedance bandwidths over the C/X/Ku/K bands. The antenna showed resonances at 5.5, 12.4, and 17.3 GHz and achieved circular polarization with axial ratio of lower than 3 dB. The numerical predictions obtained from HFSS simulations and the experimental data agreed well. However, the multi-band nature of the design spreads the electromagnetic optimization over several operating frequencies, making it more challenging to achieve high stability and tightly confined performance within a single X-band channel—a requirement that is often critical for CubeSat downlink missions [12].

2. ANTENNA DESIGN

2.1. Basic Antenna Structure

The proposed antenna is a microstrip patch antenna that has a conductive ground plane underneath a metallic radiating element printed on a dielectric substrate. The ground plane guarantees field stability and forward-directed radiation, the substrate regulates electromagnetic propagation through its dielectric properties, and the patch controls the radiation characteristics. A feeding structure that has been modified to provide the necessary impedance is used to excite the antenna.

2.2. Design Equations

The fundamental equations for microstrip patch design are given below.

$$\varepsilon_{efc} = \frac{\varepsilon_r+1}{2} + \frac{\varepsilon_r-1}{2}\left[1 + 12\frac{g}{w_p}\right]^{-0.5} \quad (1)$$

$$\Delta L = 0.412g\frac{(\varepsilon_{efc}+0.3)\left(\frac{W_p}{g}+0.264\right)}{(\varepsilon_{efc}-0.258)\left(\frac{W_p}{g}+0.8\right)} \quad (2)$$

$$W_p = \frac{C}{2f_r\sqrt{\frac{\varepsilon_r+1}{2}}} \quad (3)$$

$$L_{efc} = \frac{C}{2f_r\sqrt{\varepsilon_{efc}}} \quad (4)$$

$$L_p = L_{efc} - 2\Delta L \quad (5)$$

In these formulas The resonant frequency is represented by f_r, the substrate dielectric constant byε_r, the substrate thickness by g, the patch width by W_p, the effective dielectric constant byε_{efc}, the length extension caused by fringing fields byΔL, the effective patch length byL_{efc}, and the final physical length of the patch by L_p [13].

2.3. Proposed Antenna Design

An FR-4 substrate with a substrate thickness of 1.6 mm, a dielectric constant of 4.3, and a copper ground plane thickness of 0.027 mm was used to design the proposed antenna. For X-band CubeSat applications, the antenna shape is based on a small microstrip patch design. In order to improve the resonant characteristics and radiation performance without increasing structural complexity, controlled geometric modifications were introduced through apertures etched in radiating patch. A microstrip feed line was utilized to achieve appropriate impedance matching, The geometrical specifications of the suggested antenna are listed in *table 1*, While the ground plane, patch-substrate arrangement, side view, and final antenna layout are a geometrically presented in *figure 1*.

Table 1. Geometrical parameters of the proposed X-band patch antenna made of microstrip

Geometrical Parameters	Value(mm)
Width of Patch (W_p)	11
Length of Patch (L_p)	16
Width of Ground (W_g)	20
Length of Ground (L_g)	24
Width of Feed (W_f)	1.65
Length of Feed (L_f)	4
Thickness of Substrate (g)	1.6
Thickness of Ground (r)	0.027

FOREX Publication
Open Access | Rapid and quality publishing
International Journal of Electrical and Electronics Research (IJEER)
Research Article | Volume 14, Issue 2 | Pages 343-350 | e-ISSN: 2347-470X

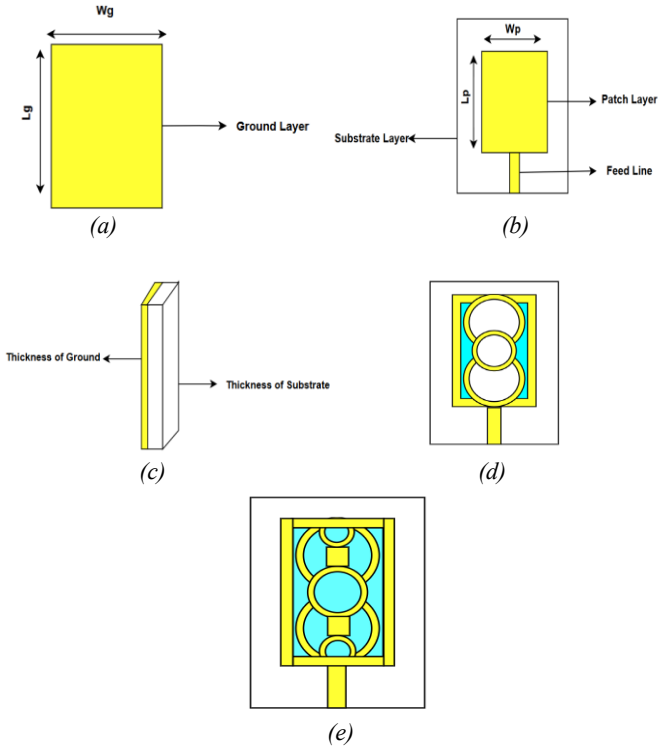

Figure 1. Geometry of Proposed antenna (a)Ground Plane, (b) Patch-Substrate Configuration, (c) Side View and (e) Proposed Antenna Structure

2.4. Modified Antenna Design

The Proposed structure was modified geometrically. By eliminating the lateral patch frame and changing the feed-line width in the design illustrated in *figure 2*. The suggested method merely employs intrinsic geometric alteration and improves performance without adding more structural complexity, in contrast to traditional methods that depend on active switching components, multilayer structures, or parasitic elements. Furthermore, the suggested approach preserves minimal complexity, which improves the antenna's dependability, ease of fabrication, and suitability for CubeSat limitations.

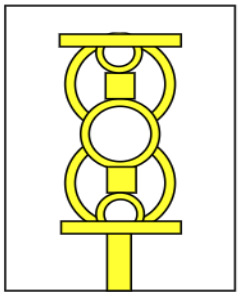

Figure 2. Modified Antenna

2.5. Equivalent Circuit of the Modified Antenna

The equivalent circuit of the modified antenna is produced by examining the electromagnetic characteristics of the suggested antenna, as illustrated in *figure 3*. A parallel RLC equivalent circuit connected in parallel to the feeding network can be used to mimic the antenna's single resonant mode at 12.232 GHz. The metallic loops and current pathways form the inductance L_r, while the coupling gaps and parasitic capacitance between the radiating element and the ground plane create the capacitances C_r, and C_p, respectively. The coupling gap between adjacent metallic parts creates the capacitance C_r, while the parasitic capacitance between the radiating element and the ground plane creates the capacitance C_p. The following relationship can be used to get a reliable approximation of the resonant frequency;

$$f_r = \frac{1}{2\pi\sqrt{L_r C_r}} \quad (6)$$

The inductive and capacitive reactance can also be expressed as follows;

$$X_C = \frac{1}{2\pi f_r C} \quad (7)$$

$$X_L = 2\pi f_r L \quad (8)$$

The resonance feature of the suggested antenna is that as the frequency increases, the inductive reactance increases and the capacitive reactance decreases. Additionally, the inductance's path lengthens with the effective current path, and the capacitance increases with the electromagnetic coupling between the metallic components. Additionally, R_s represents the usual 50Ω feeding port, and R_r represents the radiation and conduction loss. The good agreement between the simulated S11 response and the suggested RLC model validates the validity of the proposed equivalent circuit to mimic the behavior of the improved antenna.

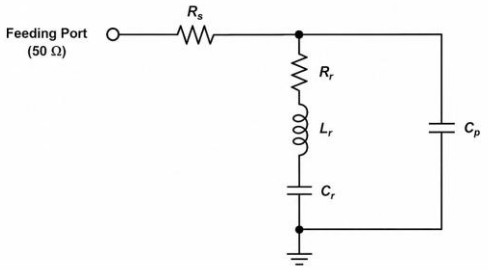

Figure 3. The proposed RLC equivalent circuit model of the modified single-band antenna

3. RESULTS AND DISCUSSION

CST Studio Suite software to analyze the performance of the proposed and modified antenna structures. The reflection coefficient (S11), gain, directionality, radiation characteristics, and impedance matching were used to assess the simulation findings. To illustrate the improvement made for CubeSat applications in the X-band, the impact of the introduced geometric alterations on antenna performance was also examined and contrasted.

Table 2. shows the performance comparison of the proposed antenna for various feedline widths

Change Width of Feed (mm)	Fr (GHz)	S11 (dB)	G (dBi)	Z11 (Ω) Z11(Ohm)	D (dBi)	VSWR
1.65	11.347	-20.06	-0.429	53.878	5.234	1.22
	12.809	-54.92	3.688	48.68	6.38	1.004
1.45	11.336	-18.81	-0.539	70.28	5.19	1.21

FOREX Publication
Open Access | Rapid and quality publishing
International Journal of Electrical and Electronics Research (IJEER)
Research Article | Volume 14, Issue 2 | Pages 343-350 | e-ISSN: 2347-470X

	13.02	-57.03	2.25	54.07	5.86	1.06
1.3	11.32	-16.07	-0.536	75.09	5.197	1.011
	12.68	-38.3	3.207	50.15	6.86	1.22
1.2	11.33	-17.4	-0.54	70.44	5.18	1.315
	12.66	-36.11	3.27	68.64	6.95	1.16
1	11.32	-16.07	-0.536	97.56	5.19	1.38
	12.61	-29.45	3.43	60	7.18	1.22

As seen in *figure 4* and summed up in *table 2*, the suggested antenna underwent a parametric study of the feedline width to examine how this parameter influences several performance aspects such reflection coefficient S11, impedance matching, gain, directivity, and VSWR. Because the input impedance of the suggested structure varies with feedline width, the results showed that the resonant characteristic and matching performance of the antenna may be directly controlled by changing the feedline width. The ideal feedline width for minimizing the reflection coefficient and producing consistent impedance matching around the target resonant frequency was determined to be 1.65mm. In order to create the modified antenna in this study, this configuration was selected as the reference configuration.

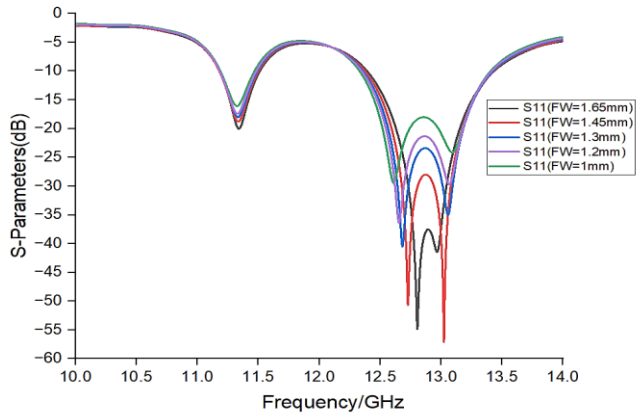

Figure 4. The proposed antenna's simulated reflection coefficient S11 with varying feedline

Table 3. This is a comparison of the proposed antenna's performance using various substrate materials

Type of material	ε_r	Fr (GHz)	S11 (dB)	G (dBi)	Z11 (Ω) Z11 (Ohm)	D (dBi)	VSWR
FR-4 (lossy)	4.3	11.347	-20.06	-0.429	53.878	5.234	1.22
		12.809	-54.92	3.688	48.68	6.38	1.004
Rogers TMM6 (lossy)	6.3	10.76	-18.32	2.99	67	4.79	1.27
Rogers RO4350 B(lossy)	3.66	2.19	-21.99	3.28	70.75	5.35	1.18
		13.69	-36.33	6.06	69.18	7.38	1.03
PTFE (lossy)	2.1	11.88	-9.81	6.45	68.7	7.93	1.95
Arlon AD 3000D	6.15	10.913	-18.18	2.96	67.9	4.89	1.68

According to *table 3*, the FR4 antenna has the highest balanced overall performance for fixed antenna dimensions. With good impedance matching properties and robust resonance behavior, the suggested FR4 antenna was able to sustain the intended dual-band operation in the X-band. While the gain and directivity of certain other substrate material types improved, they were unable to maintain the proper dual-band response or resonance shift outside of the intended working range. Additionally, it was discovered that the FR4-based geometry significantly improved the reflection coefficient S11, confirming both the viability of FR4 for the suggested antenna structure and the efficacy of the suggested geometrical adjustments.

3.1. Baseline Dual-Band Antenna Performance

The proposed antenna employs a modified microstrip patch configuration to facilitate dual-band functionality inside the X-band spectrum. The antenna design facilitates good control of current pathways without augmenting structural complexity. The simulated S11 response depicted in *figure 5*. reveals two resonant frequencies at 11.347 GHz and 12.809 GHz, both beneath the -10 dB matching threshold, hence affirming effective impedance matching and stable dual-band functionality.

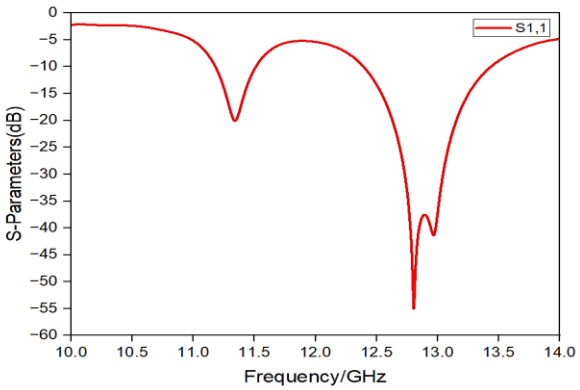

Figure 5. X-band microstrip patch antenna with dual band resonant behavior in the X-band frequency range and its simulated reflection coefficient (S11)

Figure 6 illustrates the surface current flow distribution of the suggested antenna at two distinct resonance frequencies, indicating various excitation modes in the antenna form. The effective current path is longer and resonance happens at a lower frequency because the surface current is primarily in the outer frame and the feed-line area at the frequency of 11.347 GHz. However, it is evident that the current is focused in the middle and inner regions of the structure at 12.809 GHz, which lowers the effective current path and permits resonance at a higher frequency.

(a) *(b)*

Figure 6. Surface current distribution at frequencies (a) 11.347 GHz and (b) 12.809 GHz on the surface of the suggested antenna

FOREX Publication
Open Access | Rapid and quality publishing
International Journal of Electrical and Electronics Research (IJEER)
Research Article | Volume 14, Issue 2 | Pages 343-350 | e-ISSN: 2347-470X

Figure 7 displays the simulated radiation patterns at the two resonant frequencies. Due to improved field confinement, the antenna exhibits a more concentrated radiation beam at 12.809 GHz with higher directivity and current concentration. At 11.347 GHz, the antenna exhibits a wider radiation beam with moderate directivity. This result confirms that the proposed design can enable stable dual-band operation with enhanced radiation performance across the X-band. *Table 4* summarizes the results of the Proposed antenna performance parameters.

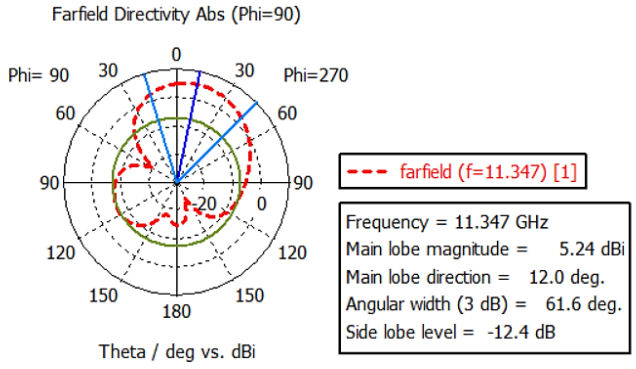

(a)

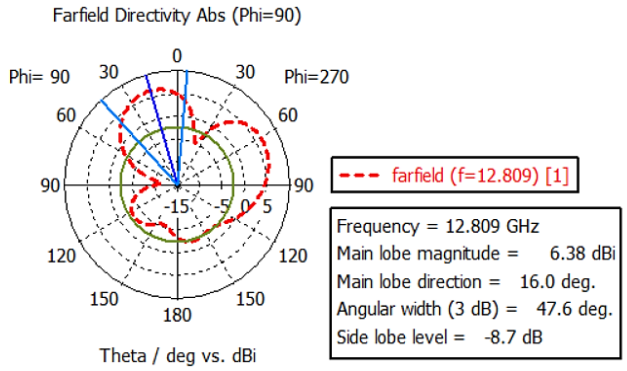

(b)

Figure 7. Two-dimensional patterns of radiation of the baseline antenna at (a) 11.34 GHz and (b) 12.809 GHz, respectively which are the first and second modes of resonance, respectively

Table 4. Theoretical values of impedance and radiation performance of the dual-band X-band microstrip patch antenna at the resonant frequencies

Fr (GHz)	S11 (dB)	G (dBi)	Z11 (ohm)	D (dBi)	BW (GHz)	VSWR
11.347	-20.06	-0.429	53.878	5.234	0.335	1.22
12.809	-54.92	3.688	48.86	6.38	1.03	1.004

3.2. Modified Single-Band High-Directivity Configuration

The modified antenna configuration is obtained by changing the feed line and removing the lateral frame surrounding the patch. These geometric modifications, based on resonant-mode control via geometric reshaping, significantly alter the electromagnetic behaviour of the antenna. The simulated S_{11} response presented in *figure 8*. a single dominant resonance at 12.232 GHz, with a reflection coefficient of −32.97 dB, indicating excellent impedance matching. The lower-frequency resonance observed in the baseline design is effectively suppressed.

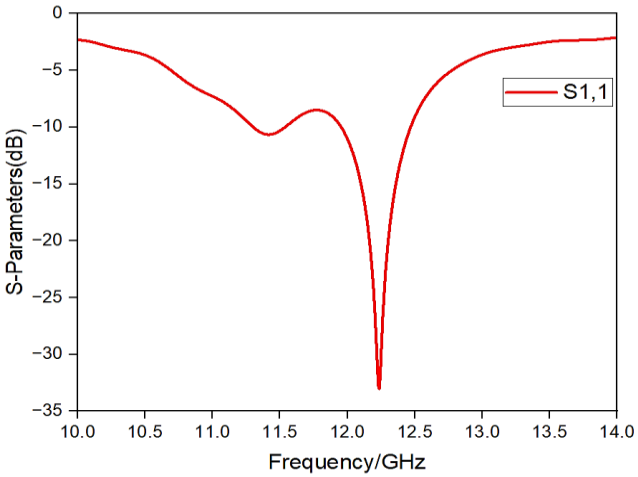

Figure 8. The magnitude of the simulated reflection coefficient (S 11) of the modified X-band single-band X-band microstrip antenna

The surface current distribution, shown in *figure 9*, reveals that electromagnetic energy is now concentrated along a well-defined radiating path, with minimal current presence in the regions where the lateral frame was removed. This confirms that the geometric modification successfully suppresses undesired resonant modes and stabilizes a single dominant mode.

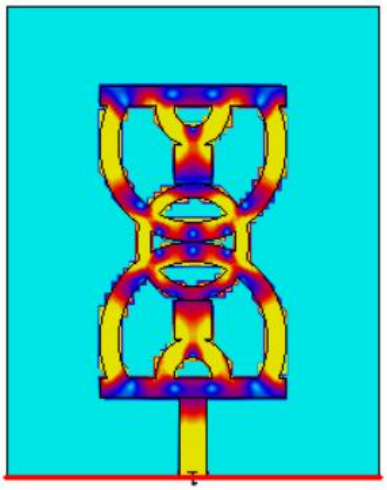

Figure 9. show the surface current distribution of the modified single-band antenna when it is working at a frequency of 12.232 GHz

As a result, the radiation pattern becomes more concentrated, improving directivity to 9.30 dBi. This results from an efficient primary current flow radiator, improved field concentration, and less energy spread. *Figure 10* displays the modified antenna's simulated radiation pattern. For point-to-point communication lines, which need reliable single frequency operation and strong directivity, this is especially appropriate summarizes the results of the modified antenna performance parameters in *table 5*.

FOREX Publication
Open Access | Rapid and quality publishing
International Journal of Electrical and Electronics Research (IJEER)
Research Article | Volume 14, Issue 2 | Pages 343-350 | e-ISSN: 2347-470X

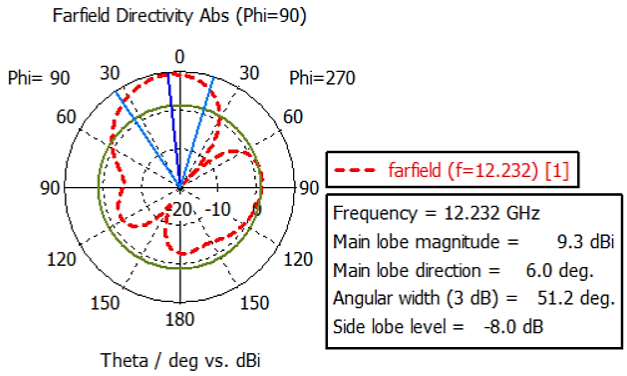

Figure 10. The revised antenna's two-dimensional Farfield radiation pattern at its resonance frequency (12.232 GHz)

Table 5. Theoretical values of impedance and radiation performance of the single-band X-band microstrip patch antenna at the resonant frequencies

Fr (GHz)	S11 (dB)	G (dBi)	Z11 (ohm)	D (dBi)	BW (GHz)	VSWR
12.232	-32.97	4.506	55.17	9.305	0.58	1.16

3.3. Performance Trade-Off and Design Implications

The findings reveal a basic trade-off between small microstrip antenna radiation directivity and frequency diversity. The dual-band baseline architecture offers coverage at lower frequencies and flexibility in communications. The improved directivity and radiation efficiency of the new design come at the expense of multi-band capabilities. This work's primary contribution is demonstrating how geometric reshaping may be used to systematically control this trade-off without adding more parts or increasing the design's complexity. This method is ideal for CubeSat systems with size and reliability limits since it offers an easy and effective way to customize the antenna performance.

4. COMPARISON OF THE PROPOSED AND MODIFIED ANTENNA DESIGNS WITH EXISTING SATELLITE ANTENNA DESIGNS

The suggested antenna's efficacy is contrasted with newly released satellite and CubeSat antenna designs. Operating frequency, bandwidth, gain, and impedance matching are all compared, as summarized in Table 6. The baseline antenna exhibits strong impedance matching at both resonant frequencies and good dual-band performance in the X-band. When compared to some of the stated designs, the reflection coefficient of −54.92 dB at 12.809 GHz is excellent. With a directivity of 9.30 dBi at 12.232 GHz, the improved construction outperforms several tiny X-band reported antennas. In contrast to many current methods that call for: Electromagnetic bandgap (EBG) structures Parasitic components. By just making geometrical changes in one or more layers, the suggested design enhances performance. As a result, the construction is more straightforward, easier to fabricate, and more dependable. Although some known designs reach higher gain, they frequently call for larger antenna arrays or several layers, which are impractical in a CubeSat's extremely limited surroundings. However, because the suggested antenna design is single-layer and compact, it is better suited for small satellite platforms.

Table 6. Comparison of the Proposed and Modified Antenna with Reported Satellite Antenna Designs Performance

Reference	Antenna Type	Fr	BW	S11 (dB)	Type of Band	G (dBi)
[14]	SIW-Based Slot Antenna	11.8GHz	342.7MHz	-17.74	X- Band	4.29
[15]	LC-loaded Dual-Band Monopole	144MHz	6MHz	<-10	VHF-Band	2.14
		435MHz	30MHz	<-10	UHF-Band	4.35
[16]	SIW Cavity-Backed Slot Antenna	11.9GHz	1.8GHz	-23	X- Band	8.5
[17]	Dual-band stacked microstrip patch antenna	2.05GHz	85MHz	-25	S-Band	6.55
		8.30GHz	2.4GHz	-30	X-Band	12.5
This Work	microstrip patch antenna	11.34GHz	0.335GHz	-20.06	X-Band	-0.429
		12.809GHz	1.03GHz	-54.92		3.688
Modified Work		12.232GHz	0.58GHz	-32.97		4.506

International Journal of
Electrical and Electronics Research (IJEER)
Research Article | Volume 14, Issue 2 | Pages 343-350 | e-ISSN: 2347-470X

5. CONCLUSION

In this paper, a small X-band microstrip patch antenna for CubeSat communication applications is presented. A new method of performance reconfiguration is presented, which is based on resonant-mode control via geometric reshaping without increasing complexity of structural. The baseline antenna was found to have steady radiation characteristics and good impedance matching. It was planned to operate in two bands, at 11.347 GHz and 12.809 GHz. The directivity was subsequently increased to 9.30 dBi by reconfiguring the antenna as a single-band antenna at 12.232 GHz utilizing particular geometric adjustments. The findings demonstrate that it is feasible to successfully manage the resonant modes and enable a changeover between multiple band and high-directivity modes in the same antenna structure by applying controlled geometric modifications to the antenna. By doing away with the requirement for additional parts, this design streamlines the system, improving dependability and compatibility with CubeSat platforms. In order to further enhance gain capabilities for long-range communication systems on CubeSats in the future, this concept will be expanded to antenna array topologies and validated experimentally.

REFERENCES

[1] Y. S. Gurbet and S. Doğu, "Comprehensive Review of Ku, K, and Ka Band Antenna Designs: Applications in CubeSats," International Journal of Aeronautical and Space Sciences, vol. 26, no. 2, pp., Jun. 2025, doi: 10.1007/s42405-025-00989-5.

[2] Z. Mashayekh Bakhsh, Y. Omid, G. Chen, F. Kayhan, Y. Ma, and R. Tafazolli, "Multi-Satellite MIMO Systems for Direct User–Satellite Communications: A Survey," IEEE Communications Surveys & Tutorials, vol. 26, no. 3, pp. xxx–xxx, Jul. 2024, doi: 10.1109/COMST.2024.3376961.

[3] H. I. Hamd, I. H. Ali, and A. M. Ahmed, "Design and simulation double Ku-band Vivaldi antenna," Indonesian Journal of Electrical Engineering and Computer Science, vol. 25, no. 1, pp. 396–403, Jan. 2022, doi: 10.11591/ijeecs.v25.i1.pp396-403.

[4] S. Abulgasem, F. Tubal, R. Raad, P. I. Theoharis, S. Liu, and S. Arumugam, "Antenna Designs for CubeSats: A Review," IEEE Access, vol. 9, pp. 45289–45324, 2021, doi: 10.1109/ACCESS.2021.3068062

[5] A. Alahmadi, M. Alqahtani, A. Alzahrani, and H. Alsharif, "A comprehensive survey of CubeSat missions and communication subsystems," IEEE Access, early access, 2025, doi: 10.1109/ACCESS.2025.3637768.

[6] H. I. Hamd, M. Al-Sultani, and Z. N. A. Al-Rawi, "Influence Different Dielectric Materials for Square Patch Antenna on RCS," IEEE, pp. 1–6, 2020.

[7] M. S. Rana, S. Hossain, S. B. Rana, and M. Mustafizur Rahman, "Microstrip patch antennas for various applications: a review," Indonesian Journal of Electrical Engineering and Computer Science, vol. 29, no. 3, pp. 1511–1519, Mar. 2023, doi: 10.11591/ijeecs. v29.i3. pp1511-1519

[8] K. Singh, M. Dhayal, and S. Dwivedi, "Design and analysis of ultra-wideband microstrip patch antenna with various conductive materials for terahertz gap," Discover Applied Sciences, vol. 6, Art. no. 224, Apr. 2024, doi: 10.1007/s42452-024-05886-2.

[9] L. P. Ta, D. Nakayama, and M. Hirose, "Design of a high-gain X-band electromagnetic band gap microstrip patch antenna for CubeSat applications," Electronics, vol. 14, no. 11, Art. no. 2216, May 2025, doi: 10.3390/electronics14112216.

[10] M. Simone, M. B. Lodi, N. Curreli, S. C. Pavone, G. Mazzarella, and A. Fanti, "Optimized design and Multiphysics analysis of a Ka-band stacked antenna for CubeSat applications," IEEE Journal on Multiscale and Multiphysics Computational Techniques, vol. 6, pp. 1–12, Aug. 2021, doi: 10.1109/JMMCT.2021.3115702.

[11] D. A. Jiménez, A. Reyna, L. I. Balderas, and M. A. Panduro, "Design of a 4 × 4 low-profile antenna array for CubeSat applications," Micromachines, vol. 14, no. 1, Art. no. 180, Jan. 2023, doi: 10.3390/mi14010180.

[12] A. Kumar, P. Attanayake, and A. Dhar, "Compact triple band microstrip patch antenna for satellite and C/X/K/Ku bands applications," Wireless Personal Communications, vol. 129, no. 1, pp. 57–70, Oct. 2022, doi: 10.1007/s11277-022-10085-6.

[13] H. El-Hakim and H. A. Mohamed, "Synthesis of a multiband microstrip patch antenna for 5G wireless communications," Journal of Infrared, Millimeter, and Terahertz Waves, vol. 44, no. 7, pp. 752–768, Aug. 2023, doi: 10.1007/s10762-023-00937-y.Title of Site. Available online: URL (accessed on Day Month Year).

[14] P. Chaurasia, R. Nigam, and M. Bhowmik, "SIW based slot antenna in X-band using Rogers RT/duroid

[15] S. A. M. Soliman, E. M. Eldesouki, and A. M. Attiya, "Analysis and design of an X-band reflectarray antenna for remote sensing satellite system," Sensors, vol. 22, no. 3, Art. no. 1166, Jan. 2022, doi: 10.3390/s22031166.

[16] H. Taher and R. Farrell, "Broadband high gain SIW cavity square slot antenna for X-band applications," in Proc. 2016 Loughborough Antennas & Propagation Conf. (LAPC), Loughborough, U.K., Nov. 2016, pp. 1–4, doi: 10.1109/LAPC.2016.7807581.

[17] D. E. Serup, R. J. Williams, S. Zhang, and G. F. Pedersen, "Shared aperture dual S- and X-band antenna for nano-satellite applications," in Proc. 14th Eur. Conf. Antennas Propag. (EuCAP), Copenhagen, Denmark, Mar. 2020, pp. 1–5, doi: 10.23919/EuCAP48036.2020.9135774.